Electronic Supplementary Information

2D/2D/2D $Ti_3C_2T_x$@TiO_2@MoS_2 Heterostructure as Ultrafast and High-sensitivity NO_2 Gas Sensor at Room-temperature

Zhuo Liu[a], He Lv[a], Ying Xie[a], Jue Wang[a], Jiahui Fan[a], Baihe Sun[a], Lin Jiang[a], Yang Zhang[a], Ruihong Wang*[a] and Keying Shi*[a]

a. Key Laboratory of Functional Inorganic Material Chemistry, Ministry of Education. School of Chemistry and Material Science, Heilongjiang University, Harbin, 150080, P. R. China.

* Corresponding author

Corresponding author: Tel.: +86 451 86609141; +86 451 86604920

E-mail: wangruihong@hlju.edu.com

E-mail: shikeying2008@163.com

Fax: +86 4518667 3647; Tel: +86 451 8660 9141

Table S1 NO_2 sensing performance of MoS_2-based sensors.

Materials	W. T. (°C)	Gas Conc. (ppm)	T_{res}/T_{rec}	Sensitivity (R_a/R_g)	LOD (ppm)	Ref
$Ti_3C_2T_x$@TiO_2@MoS_2	**RT (25°C)**	**50**	**1.8s/70.0s**	**55.12①**	**0.023**	**This Work**
p-Type MoS_2	125	100	14.33s/40.67s	10.36%②	0.1	[1]
Monolayers-MoS_2 film (visible light)	RT	0.2	83s/133s	--	0.005	[2]
MoS_2 (UV light)	RT	50	50s/100s	--	0.1	[3]
MoS_2/rGO aerogel	200	0.5	--/ < 1min	8.7%②	0.05	[4]
Few-layer MoS_2 film	120	50	--/--	38%②	--	[5]
MoS_2-ZnO	RT	50	1.5s/30.9s	~35①	0.01	[6]
MoS_2/C_3N_4 Hybrid Aerogel	RT	50	2.1s/35.7s	61.07①	0.01	[7]
MoS_2/ZnO	RT	10	--/--	40%②	--	[8]
MoS_2-rGO-Cu_2O	RT	1	--/--	3.06%②	0.08	[9]
40% 1T- and 60% 2H-MoS_2	RT	2	10s/--	25%②	0.025	[10]
MoS_2-SnO_2	RT	100	2.2s/225s	34.67①	0.5	[11]
MOF-derived In_2O_3/MoS_2	RT	20	152s/<179s	~28①	0.1	[12]
MoS_2 NSs/PbS QDs	RT	10	15s/62s	6.15①	1	[13]

W.T.: Working temperature; LOD: limit of detection; RT: Room temperature.

①: $S=R_a/R_g$

②: $S=|R_a-R_g|/R_a\times100\%$ or $S=|R_g-R_a|/R_a\times100\%$

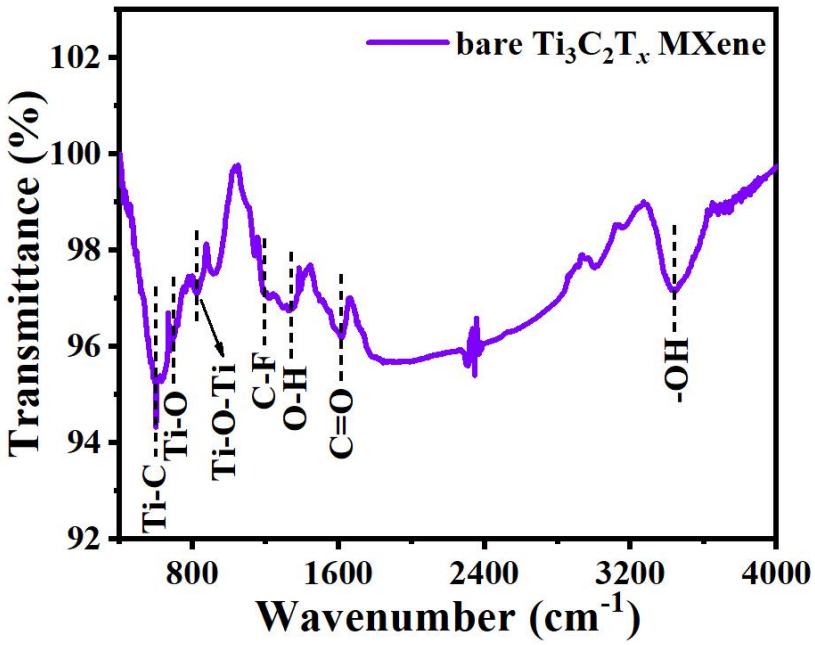

Fig. S1 FT-IR image of bare $Ti_3C_2T_x$ MXene nanosheets.

As shown in Fig. S1, FT-IR image revealed the stretching vibrations of the bare $Ti_3C_2T_x$ MXene at around 3441 and 1650 cm^{-1}, corresponding to the adsorbed water molecules (-OH) and C=O groups.[14] The peak at 1327 and at 1223 cm^{-1} are assigned to the O-H and C-F,[15] and another two obvious peaks at 601, 649 and 823 cm^{-1}, corresponding to the stretching vibration of Ti-C, Ti-O and Ti-O-Ti.[16,17]

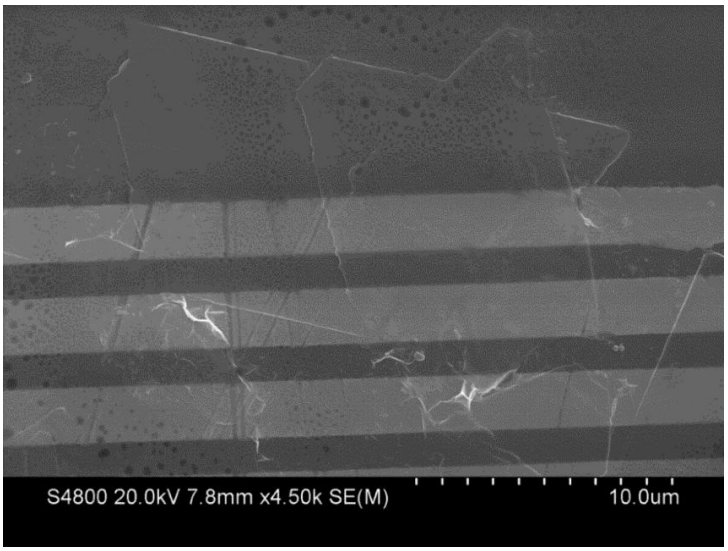

Fig. S2 SEM image of bare $Ti_3C_2T_x$ MXene nanosheets.

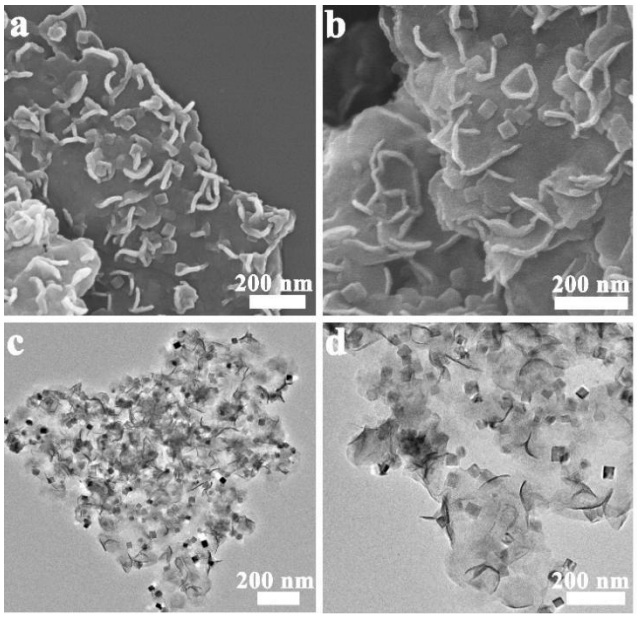

Fig. S3 SEM images of $Ti_3C_2T_x$@TiO_2@MoS_2 composite.

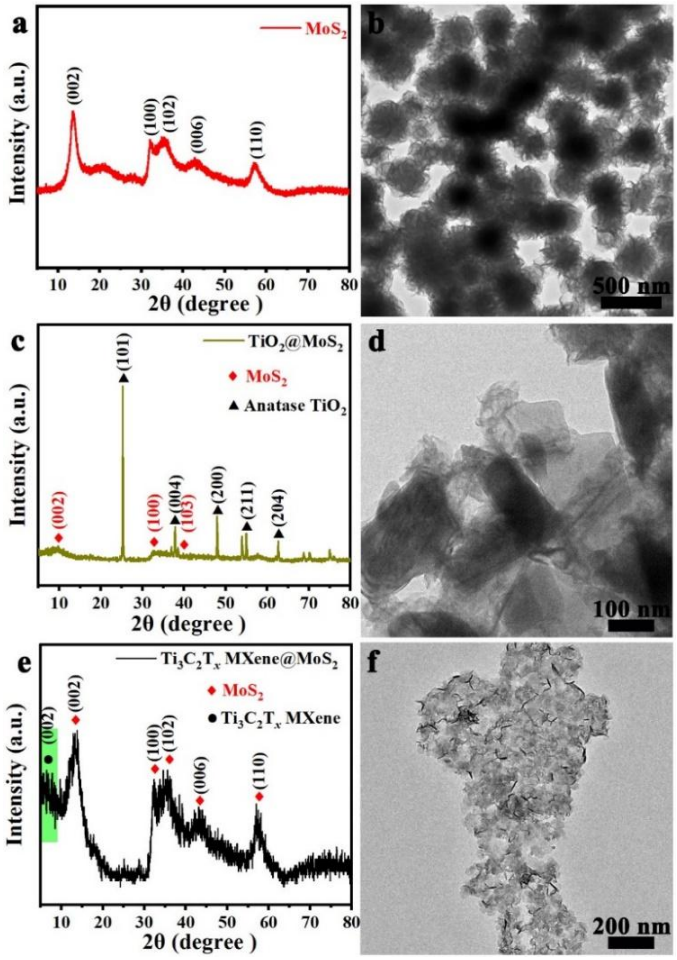

Fig. S4 (a, c and e) XRD patterns and (b, d and f) TEM images of the pristine MoS_2, TiO_2@MoS_2 and $Ti_3C_2T_x$@MoS_2 composites.

Generally, MoS_2 mainly exists in two different polymorphs, including trigonal prismatic semiconducting phase MoS_2 (2H-MoS_2) and octahedral metallic phase MoS_2 (1T-MoS_2). In this paper, all the synthesized MoS_2 are well matched to 2H-MoS_2, and 2H-MoS_2 is simply referred to as MoS_2. [17, 18]

For the pristine MoS_2 sample, the major XRD peaks at 13.69, 32.10, 35.66, 43.52 and 57.47° correspond to the (002), (100), (102), (006) and (110) plane of 2H-MoS_2, respectively. It shows the spherical structure assembled by MoS_2 layers, which is consistent with previous reports.[20] In the case of TiO_2@MoS_2, the XRD peaks at 25.3, 37.8, 47.9, 55.0 and 62.6° are in good agreement with anatase-TiO_2. It is noticed that the peak for TiO_2 (101) crystal plane is sharp and high in intensity, showing a good crystallinity. Fig. S4e displays the composition of $Ti_3C_2T_x$@MoS_2, in which the characteristic peak at 6.44° corresponds to the (002) crystal plane of $Ti_3C_2T_x$ MXene. Besides, it displays the similar appearance as $Ti_3C_2T_x$@TiO_2@MoS_2 but with the absence of TiO_2.

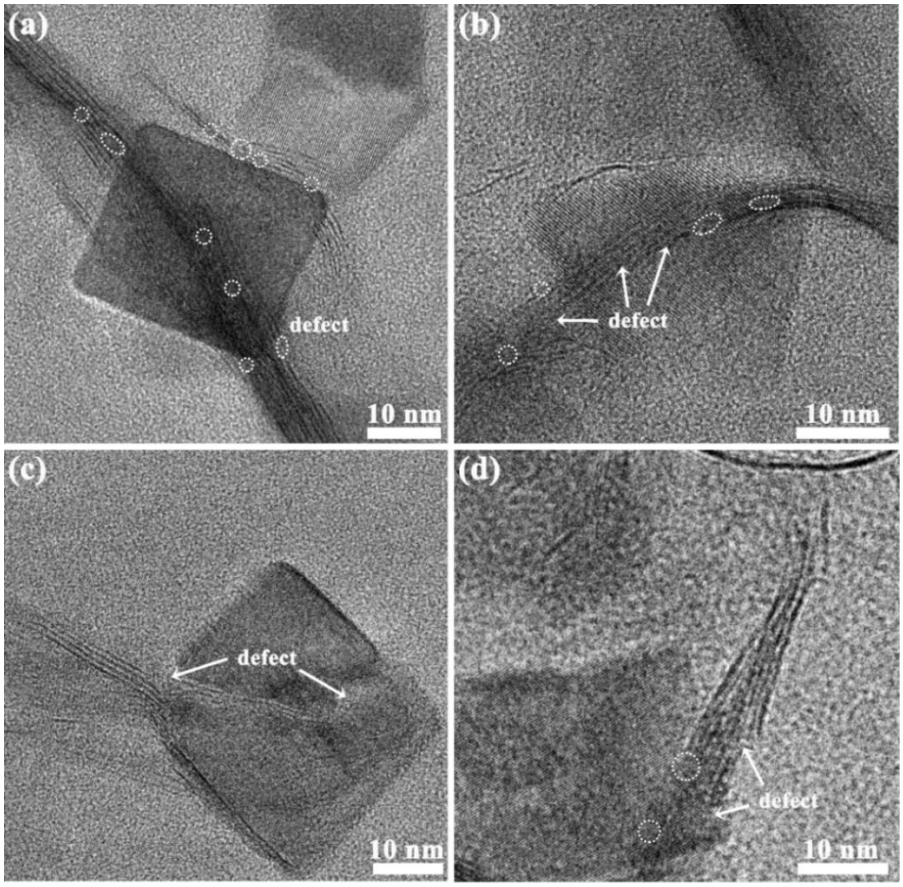

Fig. S5 (a, b) HRTEM images of $Ti_3C_2T_x$@TiO_2@MoS_2 composite (The defects were marked in white).

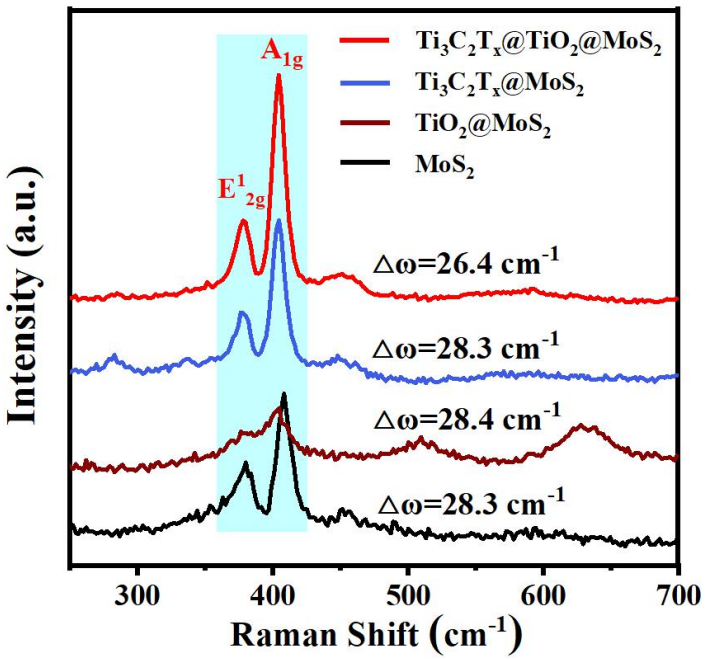

Fig. S6 Raman spectra of the $Ti_3C_2T_x$@TiO_2@MoS_2, $Ti_3C_2T_x$@MoS_2, TiO_2@MoS_2 composites and the pristine MoS_2.

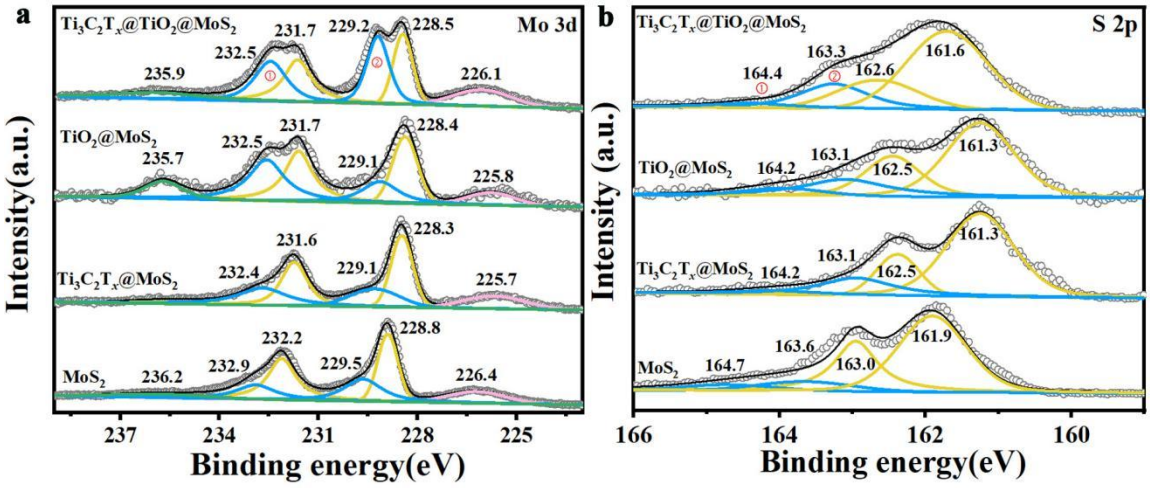

Fig. S7 XPS spectra of Mo 3d and S 2p for different samples.

Table S2 The bonding energy and peak area percent in $Mo^{5+}$and S_2^{2-} XPS spectra.

Sample	Mo^{5+} (eV)		Mo^{5+} ar.[a] (%)	S_2^{2-} (eV)		S_2^{2-} ar.(%)
	3d 3/2	3d 5/2		2p 1/2	2p 3/2	
$Ti_3C_2T_x$@TiO_2@MoS_2	232.5	229.2	41.1	164.4	163.3	24.1
TiO_2@MoS_2	232.5	229.1	38.9	164.2	163.1	23.5
$Ti_3C_2T_x$@MoS_2	232.4	229.1	34.4	164.2	163.1	22.4
MoS_2	232.9	229.5	29.8	164.7	163.6	15.2

[a] ar.% is the area percent of XPS peak. ar.% = [(area①+area②)/peak area of Mo (or S) element] ×100%

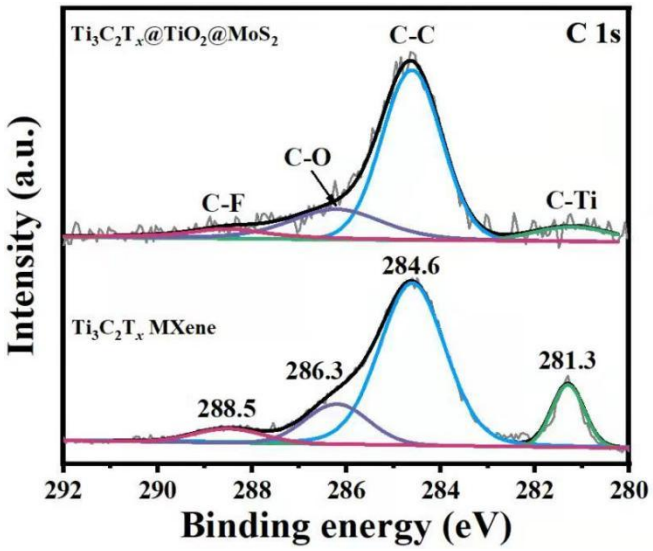

Fig. S8 The core level XPS spectrum of C 1s in $Ti_3C_2T_x$@TiO_2@MoS_2 and pristine $Ti_3C_2T_x$ MXene.

As shown in Fig. S8, the C 1s spectra is fitted by four components located at 281.3, 284.6, 286.3, and 288.5 eV, corresponding to C-Ti, C-C, C-O, and C-F bonds, respectively. It is obvious that the C-Ti decreased significantly due to the partial oxidation of $Ti_3C_2T_x$ to TiO_2.

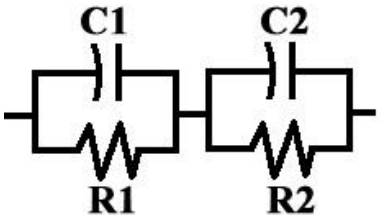

Fig S9 The equivalent circuit model used to interpret the EIS data.

Table S3 Parameters obtained by fitting experimental curve to equivalent circuit.

Raw materials	*R*1 (Ω)	*C1* (F)	*R*2 (Ω)	*C2* (F)
$Ti_3C_2T_x$@TiO_2@MoS_2	4.173×10^{5}	3.566×10^{-10}	5.712×10^{4}	5.952×10^{-11}
TiO_2@MoS_2	7.685×10^{6}	2.090×10^{-10}	2.172×10^{5}	2.368×10^{-10}
$Ti_3C_2T_x$@MoS_2	2.607×10^{5}	1.008×10^{-11}	5.935×10^{5}	3.957×10^{-10}
MoS_2	1.604×10^{5}	1.280×10^{-11}	1.493×10^{6}	7.902×10^{-10}

Table S4. The experimental conditions in detailed.

Feeding weight (g)	Molar ratio Mo:S	Hydrothermal temperature (℃)	Hydrothermal time (h)
$Na_2MoO_4•2H_2O$: 1.45 CN_2H_4S : 1.90	1:4.2	200	12
		200	**24 (optimization)**
		200	30
		180	12
		180	24
		180	30
$Na_2MoO_4•2H_2O$: 0.725 CN_2H_4S : 1.90	1:2.1	200	24
$Na_2MoO_4•2H_2O$: 1.45 CN_2H_4S : 0.95	1:8.3	200	24

Table S5 The response, response time and recovery time of different samples at RT for different NO_2 concentrations (RH: 23.4%).

Sample	Mo:S=1:4.2 200℃ 12h			Mo:S=1:4.2 200℃ 30h			Mo:S=1:4.2 180℃ 12h			Mo:S=1:4.2 180℃ 24h			Mo:S=1:4.2 180℃ 30h			Mo:S=1:2.1 200℃ 24h			Mo:S=1:8.3 200℃ 24h		
NO_2(ppm)	**S**	**T_{res}/s**	**T_{rec}/s**	**S**	**T_{res}/s**	**T_{rec}/s**	**S**	**T_{res}/s**	**T_{rec}/s**	**S**	**T_{res}/s**	**T_{rec}/s**	**S**	**T_{res}/s**	**T_{rec}/s**	**S**	**T_{res}/s**	**T_{rec}/s**	**S**	**T_{res}/s**	**T_{rec}/s**
50	14.24	8.0	38.4	13.15	3.7	62.9	20.87	6.4	61.3	35.28	9.1	62.4	18.17	8.0	100.3	45.97	2.1	74.1	42.14	3.7	95.5
30	10.94	7.5	43.2	10.08	4.8	53.3	11.45	3.2	48.5	17.92	10.1	60.3	9.44	8.5	83.2	24.12	3.7	59.2	34.63	2.1	74.7
10	4.75	8.5	35.7	7.45	4.3	50.7	5.40	5.3	46.9	4.29	9.6	52.8	8.04	9.6	85.3	2.67	4.3	64.5	3.22	4.3	66.7
5	3.68	6.4	44.8	4.19	5.9	47.5	1.63	6.4	42.2	3.43	10.1	51.2	4.83	5.9	69.3	2.24	6.9	48.0	2.19	8.0	62.4
3	3.21	5.3	45.9	3.30	6.9	46.4	1.38	7.5	39.5	3.22	8.5	51.7	4.46	9.1	67.2	1.99	7.5	56.5	1.93	9.6	54.9
1	2.56	5.9	42.7	3.06	8.0	54.9	1.30	8.5	41.1	2.72	10.1	55.5	2.07	7.5	55.4	1.63	10.7	36.8	1.73	11.2	53.3
0.5	1.93	6.9	37.9	2.28	9.6	56.0	1.21	7.4	30.9	2.48	10.7	51.8	1.41	11.2	38.9	1.58	9.6	47.5	1.51	13.9	58.7
0.3	1.71	9.1	36.3	1.65	10.7	42.1	1.15	6.9	29.9	1.39	12.8	39.5	1.20	11.7	32.5	1.35	10.1	46.9	1.33	16.5	48.0
0.1	1.57	10.7	34.7	1.23	11.2	41.6	1.08	9.6	17.1	1.28	11.2	35.2	1.15	12.3	31.5	1.14	12.8	29.3	1.29	18.7	55.5
0.05	1.22	9.0	30.4	1.09	12.8	20.3	--	--	--	1.18	14.9	29.3	--	--	--	--	--	--	1.16	20.2	43.7
0.03	1.00	11.7	22.9	--	--	--	--	--	--	--	--	--	--	--	--	--	--	--	1.10	20.8	42.1

***S: Response** **T_{res}: Response time** **T_{rec}: Recovery time**

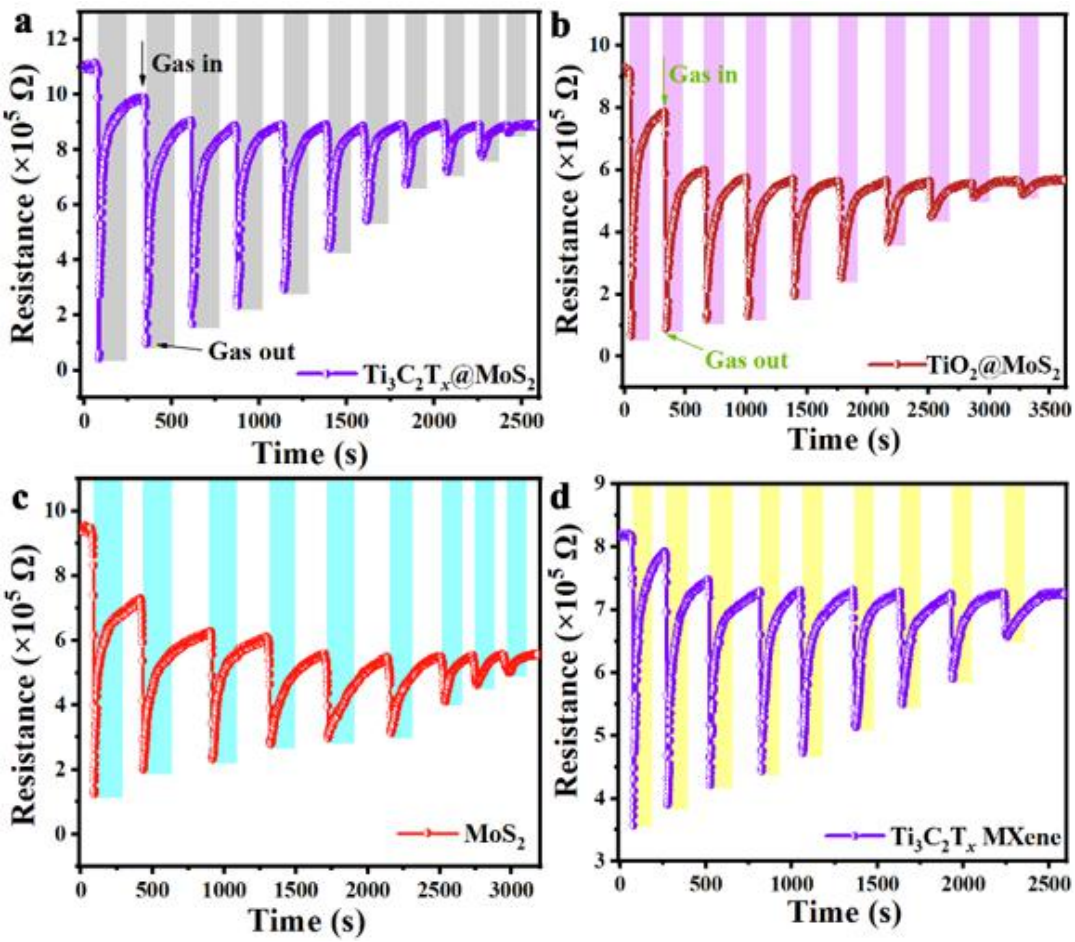

Fig. S10 Dynamic response curves of (a) $Ti_3C_2T_x$@MoS_2, (b) TiO_2@MoS_2, (c) MoS_2 and (d) $Ti_3C_2T_x$ MXene sensors to different concentration of NO_2 at room temperature (RH 23.4%).

Table S6 The response, response time and recovery time of samples at RT for different NO_2 concentrations (RH: 23.4%).

Sample	$Ti_3C_2T_x$@TiO_2@MoS_2			TiO_2@MoS_2			$Ti_3C_2T_x$@MoS_2			MoS_2		
NO_2(ppm)	S	T_{res}/s	T_{rec}/s	S	T_{res}/s	T_{rec}/s	S	T_{res}/s	T_{rec}/s	S	T_{res}/s	T_{rec}/s
50	55.16	1.8	70.0	14.46	5.5	89.6	25.67	2.1	71.2	7.59	8.5	104.8
30	22.39	2.1	62.2	8.97	6.0	87.8	10.15	2.9	65.7	3.62	9.6	98.3
10	14.34	3.2	52.5	8.41	6.5	86.2	5.38	3.2	59.0	2.64	10.1	93.9
5	8.10	3.6	49.3	5.94	6.8	84.0	4.91	3.9	53.6	2.20	12.3	141.9
3	4.46	3.9	41.8	2.74	7.9	77.6	3.04	4.6	51.5	1.88	12.8	139.7
1	2.48	5.4	40.0	2.27	9.0	76.7	2.02	6.8	42.2	1.76	14.9	126.9
0.5	1.63	6.1	36.8	1.54	9.8	79.3	1.63	7.5	37.9	1.35	13.3	90.7
0.3	1.44	6.4	34.7	1.26	10.7	72.0	1.33	8.2	36.4	1.21	15.5	66.7
0.1	1.27	7.2	32.5	1.09	11.1	66.1	1.24	8.6	34.7	1.11	17.6	63.5
0.05	1.23	7.5	30.7	1.00	11.3	49.3	1.14	9.3	32.5	--	--	--
0.03	1.17	7.9	28.9	--	--	--	1.03	10.4	29.3	--	--	--
0.023	1.08	8.6	26.8	--	--	--	--	--	--	--	--	--

***S: Response T_{res}: Response time T_{rec}: Recovery time**

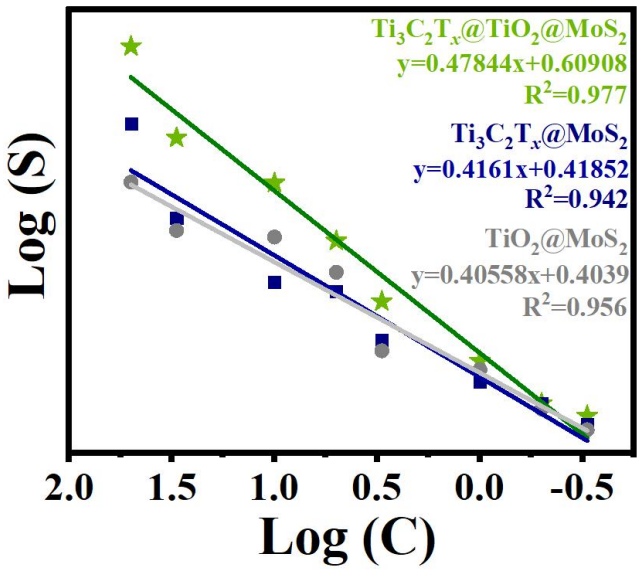

Fig. S11 The linear fitting of the $Ti_3C_2T_x$@TiO_2@MoS_2, $Ti_3C_2T_x$ @MoS_2 and TiO_2@MoS_2 sensors obtained from Fig.5a and S10a and b.

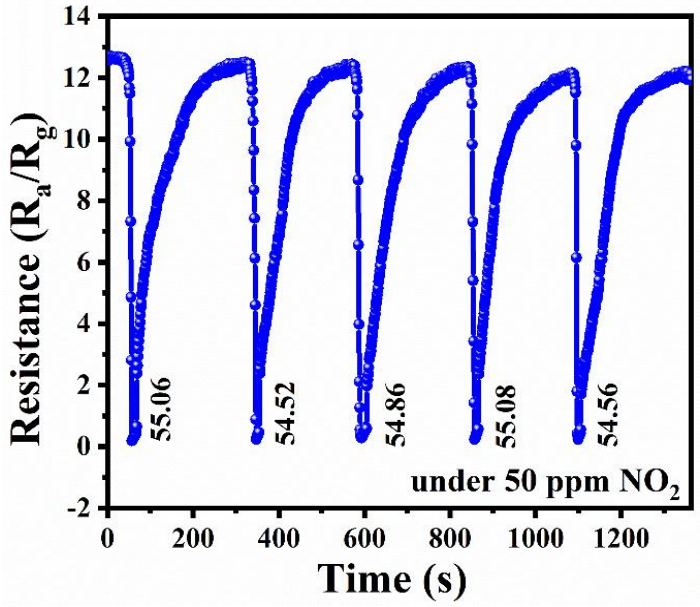

Fig. S12 Repeatability of the $Ti_3C_2T_x$@TiO_2@MoS_2 sensor to 50 ppm NO_2 with 5 circles.

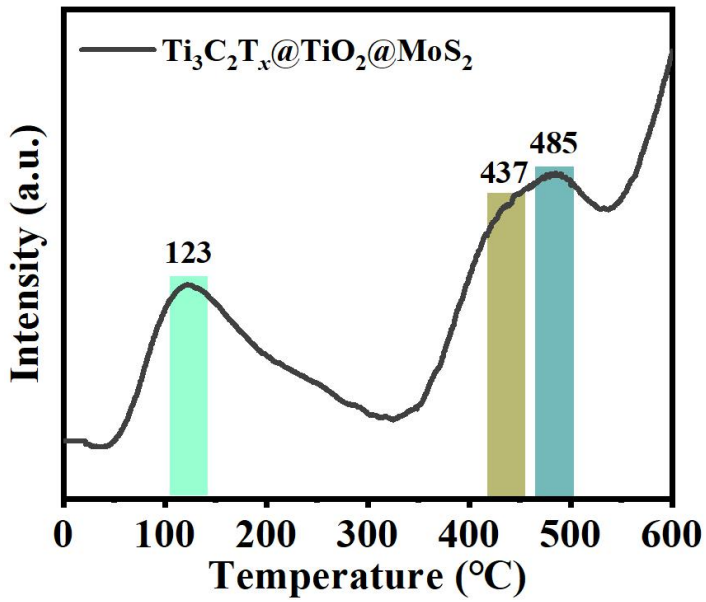

Fig. S13 NO_2-TPD of $Ti_3C_2T_x$@TiO_2@MoS_2 composite.

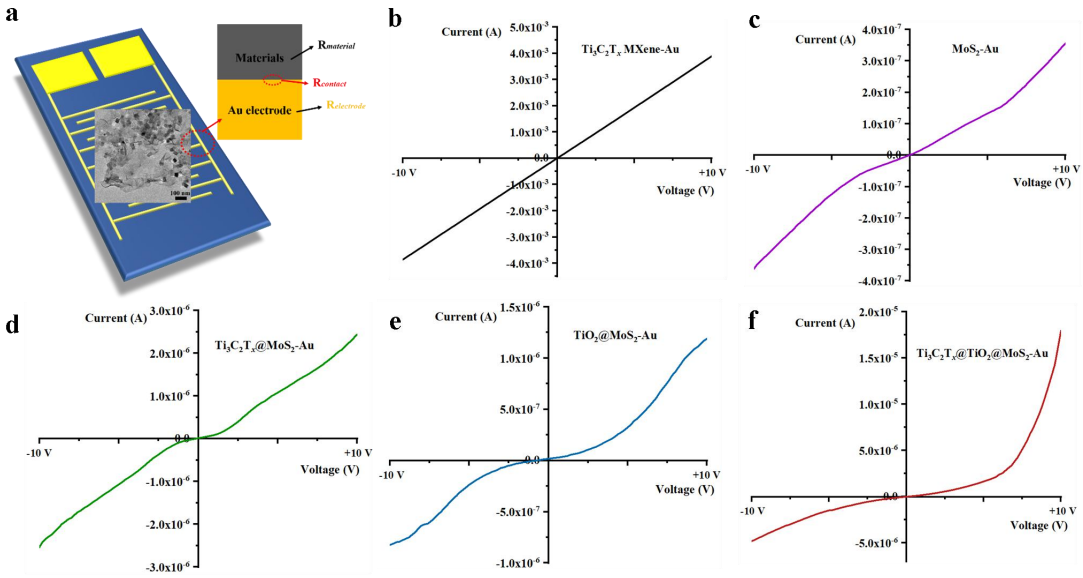

Fig. S14 The study of contact resistance: (a) gold interdigitated electrode for equivalent resistance models, and *I-V* curves of (b) $Ti_3C_2T_x$ MXene-Au, (c) MoS_2-Au, (d) $Ti_3C_2T_x$@MoS_2-Au, (e) TiO_2@MoS_2-Au, (f) $Ti_3C_2T_x$@TiO_2@MoS_2-Au.

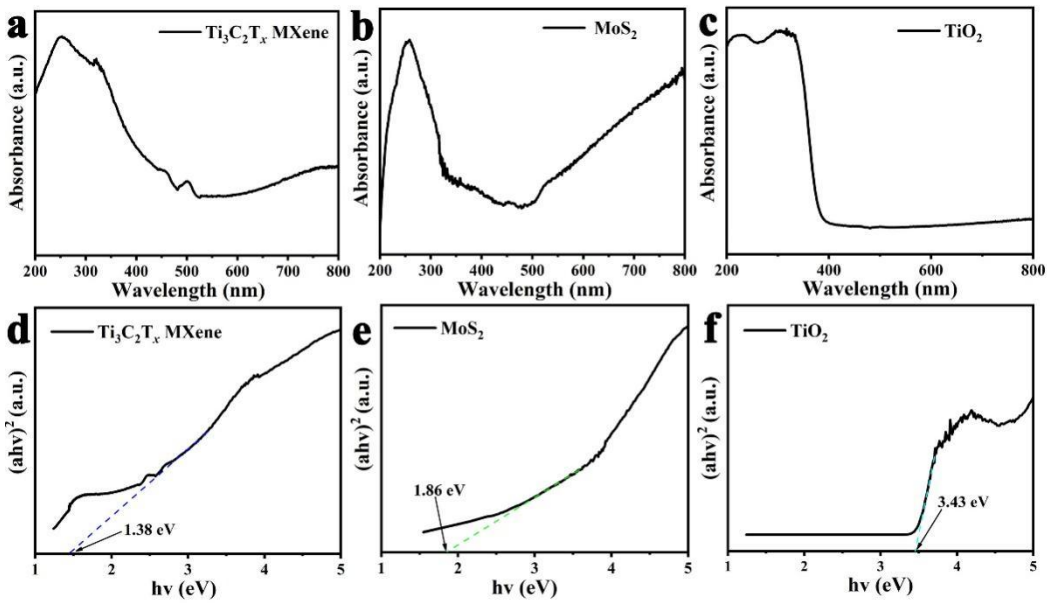

Fig. S15 (a)-(c) UV-Vis absorption spectra and (d)-(f) Tauc plots of $Ti_3C_2T_x$ MXene, MoS_2 and TiO_2. (The energy value at the point of intersection at the tangent line and the horizontal axis is the optical band gap).

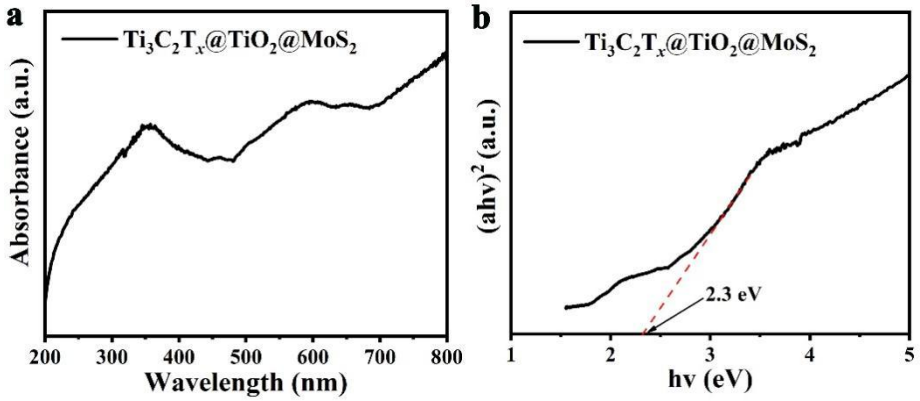

Fig. S16 (a) UV-Vis absorption spectra and (b) Tauc plots of $Ti_3C_2T_x$@TiO_2@MoS_2 composites.

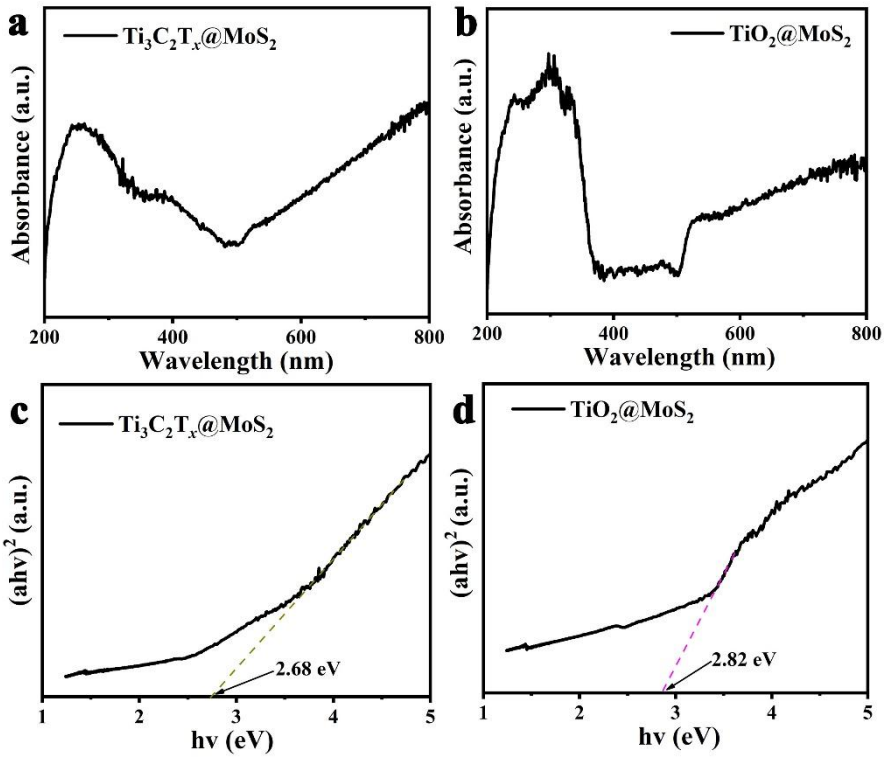

Fig. S17 (a and b) UV-Vis absorption spectra and (c and d) Tauc plots of $Ti_3C_2T_x$@MoS_2 and TiO_2@MoS_2 composites.

UV-vis analysis was conducted to further evaluate the band gaps of $Ti_3C_2T_x$ MXene, MoS_2, TiO_2, $Ti_3C_2T_x$@TiO_2@MoS_2, $Ti_3C_2T_x$@MoS_2 and TiO_2@MoS_2 composites are 1.38, 1.86, 3.43, 2.3, 2.68 and 2.82 eV respectively, which were calculated by the Kubelka-Munk method (Figure S12-17).

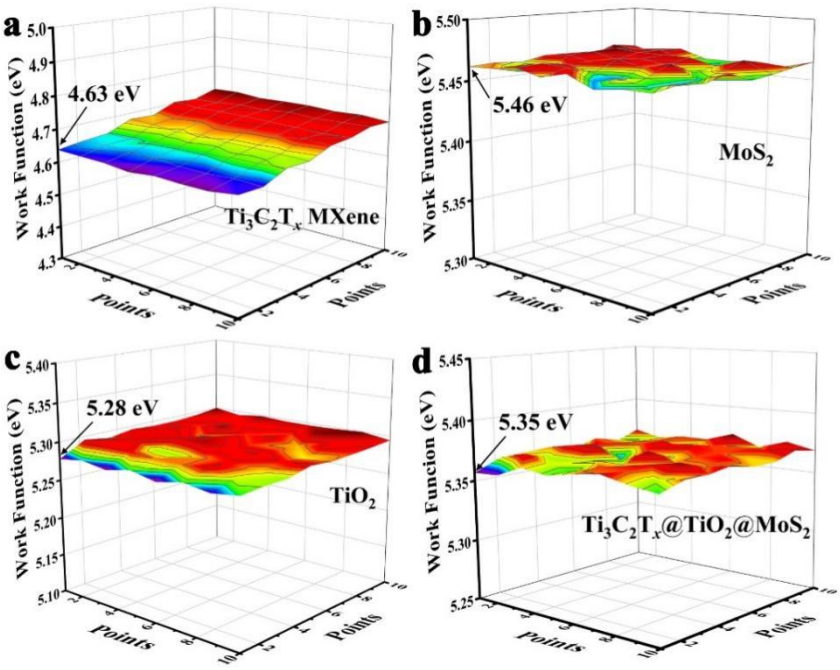

Fig. S18 (a)-(d) Scheme of the Kelvin probes of the $Ti_3C_2T_x$ MXene, MoS_2, TiO_2 and the $Ti_3C_2T_x$@TiO_2@MoS_2 hybrid composite.

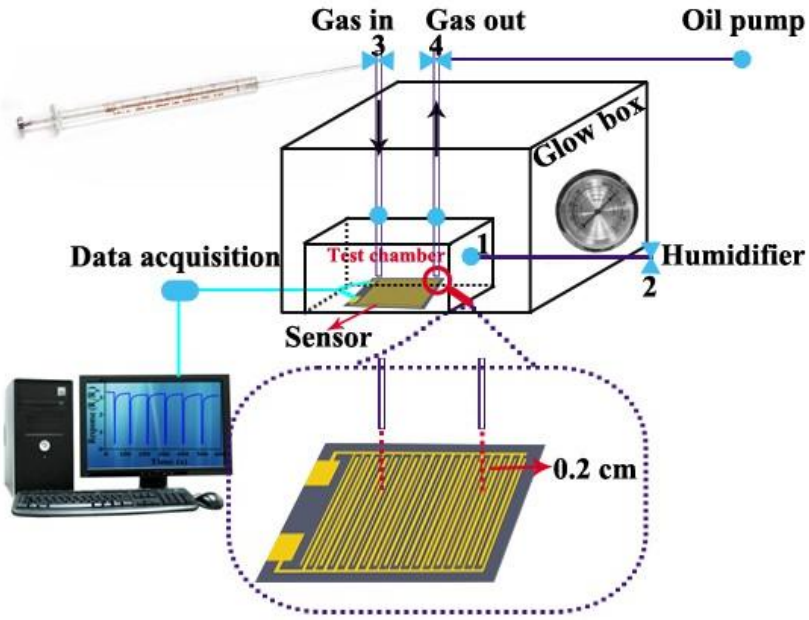

Fig. S19 The gas delivery system diagram for the sensing process.

References:

1. A.V. Agrawal, R. Kumar, S. Venkatesan, A. Zakhidov, G. Yang, J. Bao, Photoactivated mixed in-plane and edge-enriched p-type MoS_2 flake-based NO_2 sensor working at room temperature. ACS Sensors. 5 (2018) 998-1004.

2. H. Tabata, H. Matsuyama, T. Goto, O. Kubo and M. Katayama, *ACS nano*, 2021, 15, 2542-2553.6

3. W. Zheng, Y. Xu, L. Zheng, C. Yang, N. Pinna, X. Liu, J. Zhang, MoS_2 Van der Waals p-n Junctions Enabling Highly Selective Room-Temperature NO_2 Sensor, Advanced Functional Materials, 30 (2020) 2000435.

4. H. Long, A. Harley-Trochimczyk, T. Pham, Z. Tang, T. Shi, A. Zettl, C. Carraro, M. A. Worsley and R. Maboudian, *Advanced Functional Materials*, 2016, 26, 5158-5165.

5. M. Hojamberdiev, N. Goel, R. Kumar, Z.C. Kadirova, M. Kumar, Efficient NO_2 sensing performance of a low-cost nanostructured sensor derived from molybdenite concentrate, Green Chemistry, 22 (2020) 6981-6991.

6. M. Ikram, H. Lv, Z. Liu, K. Shi and Y. Gao, *Journal of Materials Chemistry A*, 2021.

7. M. Ikram, H. Lv, Z. Liu, M. Khan, L. Liu, F. Raziq, X. Bai, M. Ullah, Y. Zhang and K. Shi, *Chemistry of Materials*, 2020, 32, 7215-7225.

8. Y. Zhou, C. Gao, Y. Guo, UV assisted ultrasensitive trace NO_2 gas sensing based on few-layer MoS_2 nanosheet-ZnO nanowire heterojunctions at room temperature, *Journal of Materials Chemistry A*, 6 (2018) 10286-10296.

9. Y. Ding, X. Guo, D. Kuang, X. Hu, Y. Zhou, Y. He and Z. Zang, *Journal of Hazardous Materials*, 2021, 126218.

10. B. Zong, Q. Li, X. Chen, C. Liu, L. Li, J. Ruan, S. Mao, Highly Enhanced Gas Sensing Performance Using a 1T/2H Heterophase MoS_2 Field-Effect Transistor at Room Temperature, ACS Appl Mater Interfaces, 12 (2020) 50610-50618.

11. Y. Li, Z. Song, Y. Li, S. Chen, S. Li, Y. Li, Hierarchical hollow MoS_2 microspheres as materials for conductometric NO_2 gas sensors. Sensors and Actuators B: Chemical. 282 (2019) 259-67.

12. Z. Yang, D. Zhang and H. Chen, *Sensors and Actuators B: Chemical*, 2019, 300, 127037.

13. J. Liu, Z. Hu, Y. Zhang, H.-Y. Li, N. Gao, Z. Tian, L. Zhou, B. Zhang, J. Tang and J. Zhang, *Nano-micro letters*, 2020, 12, 1-13.

14. J. Xia, S.-Z. Yang, B. Wang, P. Wu, I. Popovs, H. Li, S. Irle, S. Dai and H. Zhu, *Nano Energy*, 2020, 72, 104681.

15. Y. Guo, T. Wang, Q. Yang, X. Li, H. Li, Y. Wang, T. Jiao, Z. Huang, B. Dong and W. Zhang, *ACS nano*, 2020, 14, 9089-9097.

16. P. Ilanchezhiyan, G. M. Kumar and T. Kang, *Journal of Alloys and Compounds*, 2015, 634, 104-108.

17. B. Dai, B. Zhao, X. Xie, T. Su, B. Fan, R. Zhang and R. Yang, *Journal of Materials Chemistry C*, 2018, 6, 5690-5697.

18. Y. Li, S. Yang, Z. Liang, Y. Xue, H. Cui and J. Tian, *Materials Chemistry Frontiers*, 2019, 3, 2673-2680.

19. D. Wang, B. Su, Y. Jiang, L. Li, B. K. Ng, Z. Wu and F. Liu, *Chemical Engineering Journal*, 2017, 330, 102-108.

20. R. Tang, D. Gong, Y. Deng, S. Xiong, J. Deng, L. Li, Z. Zhou, J. Zheng, L. Su and L. Yang, *Chemical Engineering Journal*, 2022, 427, 131809.